

# Mössbauer Study of the Magnetic Transition in $\epsilon$ -Fe<sub>2</sub>O<sub>3</sub> Nanoparticles Using Synchrotron and Radionuclide Sources

Yu. V. Knyazev<sup>a, \*</sup>, A. I. Chumakov<sup>b</sup>, A. A. Dubrovskiy<sup>a</sup>, S. V. Semenov<sup>a</sup>, S. S. Yakushkin<sup>c</sup>,  
V. L. Kirillov<sup>c</sup>, O. N. Martyanov<sup>c</sup>, and D. A. Balaev<sup>a</sup>

<sup>a</sup> Kirensky Institute of Physics, Siberian Branch, Russian Academy of Sciences, Krasnoyarsk, 660036 Russia

<sup>b</sup> European Synchrotron Radiation Facility (ESRF), F-38043 Grenoble Cedex 9, France

<sup>c</sup> Boreskov Institute of Catalysis, Siberian Branch, Russian Academy of Sciences, Novosibirsk, 630090 Russia

\*e-mail: yuk@iph.krasn.ru

Received September 26, 2019; revised October 4, 2019; accepted October 4, 2019

Nuclear  $\gamma$ -resonance experiments with energy and time resolved detection are carried out with  $\epsilon$ -Fe<sub>2</sub>O<sub>3</sub> nanoparticles and a <sup>57</sup>Co(Rh) laboratory Mössbauer source of  $\gamma$  radiation and a 14.4125 keV synchrotron radiation source on the ID18 beamline (ESRF) in the temperature range of 4–300 K. Both methods show a tremendous increase in the hyperfine field in tetrahedrally coordinated iron positions during the magnetic transition in the range of 80–150 K. As a result, the splitting of the quantum beat peaks in the nuclear scattering spectra is observed in the time interval of 20–170 ns with a periodicity of ~30 ns. In addition, the first quantum beat is slightly shifted to shorter times. A correlation between the quadrupole shift and the orbital angular momentum of iron in  $\epsilon$ -Fe<sub>2</sub>O<sub>3</sub> nanoparticles is found. The magnetic transition leads to the rotation of the magnetic moment in the tetrahedral positions of iron around the axis of the electric field gradient by an angle of 44°.

DOI: 10.1134/S0021364019210082

## 1. INTRODUCTION

Nuclear forward scattering using synchrotron radiation sources [1, 2] makes it possible to significantly expand the scope of studies of nanostructures by nuclear gamma resonance, which include traditional Mössbauer spectroscopy with a radionuclide source. Using a synchrotron radiation source, the magnetic structures of multilayer film structures were determined [3], and the spin and structural transitions in nanocrystals were studied under the application of enormous pressure (over 100 GPa) [4–6]. In addition, synchrotron radiation allows the study of materials containing isotopes rare for traditional Mössbauer spectroscopy, e.g., <sup>61</sup>Ni [7].

Nuclear forward scattering on ensembles of nanoparticles at present has been studied only in a few works primarily because such samples are three-dimensional magnets, and the study of their magnetic structure has a number of difficulties, especially if the object is a multisublattice magnet. However, to analyze the magnetic structure of  $\gamma$ -Fe<sub>2</sub>O<sub>3</sub> nanoparticles, the authors of [8] recently used the nuclear forward scattering method with the application of an external magnetic field and the field cooling regime in order to “freeze” the magnetic moment of the particles. This allowed the authors to demonstrate the canting of magnetic sublattices in  $\gamma$ -Fe<sub>2</sub>O<sub>3</sub>. In general, Fe<sub>2</sub>O<sub>3</sub> can

be crystallized in various modifications, e.g.,  $\epsilon$ -Fe<sub>2</sub>O<sub>3</sub>. This polymorphic modification can exist only on a nanoscale [9].

Thus, nuclear forward scattering can become indispensable in the study of a complex magnetic structure of  $\epsilon$ -Fe<sub>2</sub>O<sub>3</sub> [10]. An interesting transition in the range of 80–150 K was earlier found in  $\epsilon$ -Fe<sub>2</sub>O<sub>3</sub> [10, 11]. This transition was studied by various methods (including neutron diffraction) on relatively large particles with an average size of ~20–25 nm. As a result, it was shown that the magnetic transition is a consequence of structural distortions of the crystal lattice [11]. A decrease in the size of nanoparticles enhances the effect of the surface [12, 13], and this effect can be manifested most strongly during a magnetic transition. Since the nuclear  $\gamma$ -resonance methods are the most sensitive ones, their application seems to be particularly preferable for studying the possible effects during a magnetic transition.

Oxide  $\epsilon$ -Fe<sub>2</sub>O<sub>3</sub> has a complex structure consisting of two types of cation layers. In the first type, iron occupies two distorted octahedral positions (hereinafter, Fe2 and Fe3), and in the second type, iron occupies one less distorted octahedral position and one tetrahedral position (hereinafter, Fe1 and Fe4) [10, 14]. This greatly complicates the study of its magnetic structure. In our work, we used nuclear forward scat-

tering and Mössbauer spectroscopy to study the magnetic transition on nanoparticles with the  $\epsilon$ -Fe<sub>2</sub>O<sub>3</sub> structure enclosed in a xerogel matrix.

## 2. SAMPLES AND METHODS

In this work, we studied  $\epsilon$ -Fe<sub>2</sub>O<sub>3</sub> nanoparticles immobilized in a xerogel matrix with an  $\epsilon$ -Fe<sub>2</sub>O<sub>3</sub> concentration of 20 wt %. The synthesis was carried out by introducing the iron(II) salt FeSO<sub>4</sub> · 7H<sub>2</sub>O in SiO<sub>2</sub> hydrogel by diffusion exchange in an H<sub>2</sub>SO<sub>4</sub> aqueous solution (pH = 2) and it was described in detail in [15]. The prepared  $\epsilon$ -Fe<sub>2</sub>O<sub>3</sub> nanoparticles had an average diameter of 8 nm with a standard deviation of 3.4 nm.

A powder for nuclear  $\gamma$ -resonance experiments using Mössbauer spectroscopy and nuclear forward scattering was prepared by grinding the synthesized xerogel with nanoparticles embedded in it. The Mössbauer spectra of the  $\epsilon$ -Fe<sub>2</sub>O<sub>3</sub> samples were obtained on an MS-1104Em spectrometer (Research Institute of Physics, Southern Federal University) in transmission geometry with a <sup>57</sup>Co(Rh) radioactive source in the temperature range of 4–300 K using a CFSG-311-MESS closed cycle cryostat with a sample in an exchange gas (Kriotreid Ltd). The interpretation of the spectra was performed by varying the entire set of hyperfine parameters using the least squares method in the linear approximation. Nuclear forward scattering spectra were obtained at the European synchrotron radiation facility (ESRF) synchrotron in the ID18 nuclear resonance beamline (France, Grenoble) [2]. The measurements were carried out in the temperatures range from 4 to 300 K with cooling without applying an external magnetic field. Synchrotron radiation had a linear  $\sigma$  polarization.

To measure the time resolved nuclear scattering spectra on the Mössbauer <sup>57</sup>Fe isotope, which has a natural lifetime of 141 ns and the 14.4125-keV first excited nuclear level, the ESRF storage ring worked in the four-bunch mode emitting short ( $\sim 0.1$  ns) pulses with a period of 704 ns. Iron nuclei in the samples were excited by a linearly polarized Mössbauer gamma-ray beam with an energy width of  $\sim 0.7$  meV, much larger than the characteristic hyperfine splitting of nuclear levels ( $\sim 1$   $\mu$ eV). The time resolution of time-delayed reemitted  $\gamma$ -ray photons was measured with respect to the time of the detection of instantaneous electron scattering. The experimental spectra are caused by quantum beats of transitions in the hyperfine structure, which have close resonance frequencies [16]. The measurements were carried out using fast avalanche photodiode detectors [17] with a time resolution of  $\sim 1$  ns. The spectra were processed using the MOTIF program [18] taking into account the geometry of the experiment and the type of the synchrotron radiation polarization. The Fourier transform of the time spectra was used to determine the

hyperfine parameters of iron nuclei corresponding to traditional Mössbauer spectroscopy.

## 3. RESULTS

The studied samples contained only 20 wt % of  $\epsilon$ -Fe<sub>2</sub>O<sub>3</sub> nanoparticles in the nonmagnetic xerogel matrix. Thus, the technology for producing samples [15] ensured the reduction of interactions between nanoparticles; i.e., the observed magnetic transition in the range of 80–150 K is characteristic of the material itself, and zero field cooling of the sample when measuring nuclear forward scattering and Mössbauer spectroscopy spectra did not freeze magnetic moments of nanoparticles in the sample in any selected direction despite the strong magnetic anisotropy of the material [12, 19].

Time beats during nuclear forward scattering are due to the interference of radiation components corresponding to six magnetically split <sup>57</sup>Fe sublevels (six Mössbauer allowed transitions  $\Delta m = 0, \pm 1$ ). In this case, the shape of the spectra is determined by the magnetic state of the iron nuclei in the sample. In addition, the time spectra are sensitive to the direction of the magnetization of the sample. In the case of a three-dimensional magnet, which corresponds to the equiprobable distribution of magnetic moments of all nanoparticles in space, all six nuclear sublevels are excited, and the time spectrum is determined by the interference of all frequencies of the allowed transitions. The measured nuclear forward scattering spectra are shown in Fig. 1.

The magnetic moment of all nanoparticles is locked at 4 K and the spectrum is simulated well by a four-sublattice magnet with an equiprobable distribution of Fe<sup>3+</sup> cations [10, 12, 19, 20]. However, at increasing temperature, the magnetic moment of nanoparticles is unlocked because the anisotropy energy of a particle of a certain volume is not enough to hold the moment under the effect of the thermal energy of fluctuations and the Néel–Brown relation  $T_B = K_{\text{eff}}V/\ln(\tau_0/\tau)k_B$  is fulfilled [21]. The excess of the thermal energy over magnetic energy occurs at  $T_B$  and leads to the transition of particles to a superparamagnetic state, which is manifested in nuclear forward scattering spectra as the modulating frequency of the quantum beat signal. The presence of such an envelope can be clearly seen in the spectrum at 280 K in the time interval of 70–170 ns. The superparamagnetic behavior of the particles appears as a quadrupole doublet in the Mössbauer spectra (Fig. 2), the line intensity of which increases significantly when the sample is heated. We considered superparamagnetism of  $\epsilon$ -Fe<sub>2</sub>O<sub>3</sub> nanoparticles using Mössbauer spectroscopy in detail in [13].

Excluding the features of nuclear forward scattering spectra associated with superparamagnetism of particles, the diagram of quantum beats at different

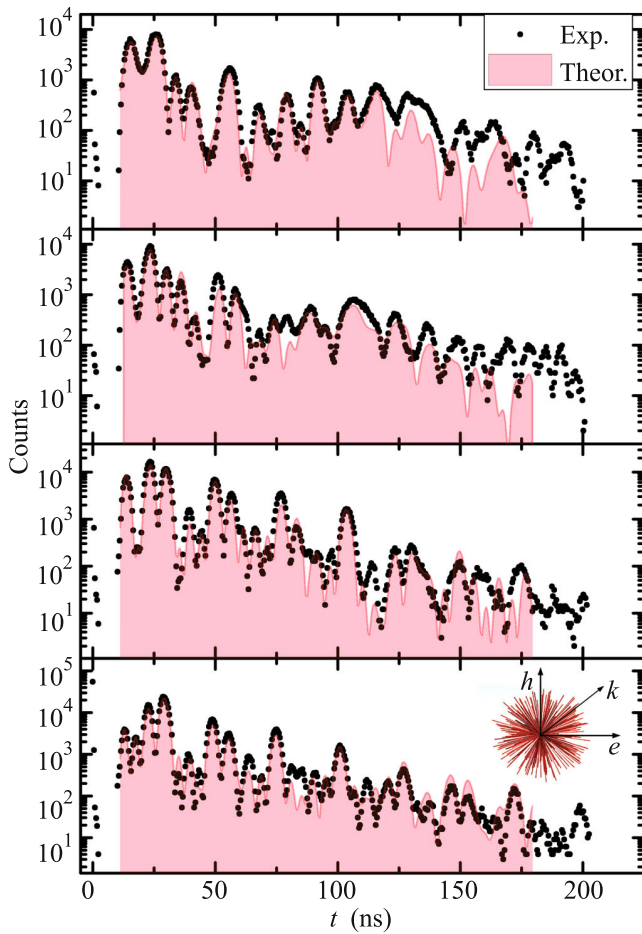


**Fig. 1.** (Color online) Nuclear gamma-resonance spectra of  $\epsilon$ - $\text{Fe}_2\text{O}_3$  nanoparticles in the temperature interval of 4–300 K. Spectra were processed in the approximation of the 3D distribution of magnetic moments of nanoparticles and the results are shown by shaded regions.

temperatures generally has a similar pattern. We can highlight some characteristic changes in the details of the spectra. First of all, this concerns the change in the intensity of nuclear decay because of the magnetic transition in the range of 80–150 K. The most characteristic changes in the intensity during a magnetic transition occur at characteristic times of  $\sim 20$ ,  $\sim 40$ ,  $\sim 70$ , and  $\sim 120$  ns. In addition, the time of the maximum of the first beat at different temperatures varies and it has the smallest value below the temperature of the completion of the magnetic transition of 80 K.

The treatment of nuclear forward scattering spectra of  $\epsilon$ - $\text{Fe}_2\text{O}_3$  nanoparticles is complicated by a large number of nuclear scattering parameters. To simplify the fitting procedure, the results of processing the Mössbauer spectra were used (Fig. 2). The chemical shifts of the  $\epsilon$ - $\text{Fe}_2\text{O}_3$  sublattices and quadrupole doublet parameters corresponding to particles with unlocked magnetic moment from the data of traditional Mössbauer spectroscopy were used. Constraints

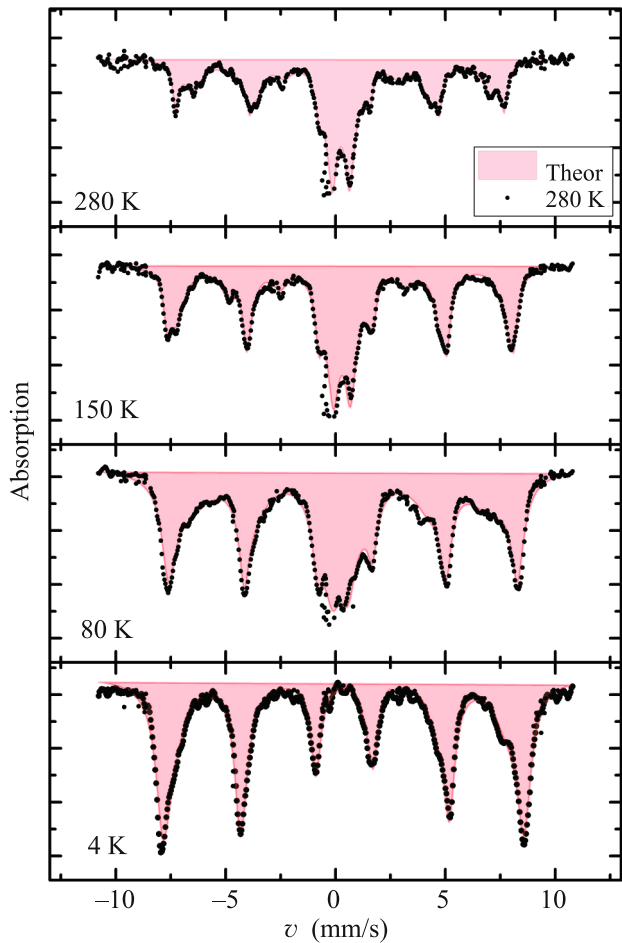


**Fig. 2.** (Color online) Mössbauer spectra of  $\epsilon$ - $\text{Fe}_2\text{O}_3$  nanoparticles in the temperature range of 4–300 K. The result of processing the spectra is shown by shaded regions.

were imposed on the remaining hyperfine parameters for the adopted model to remain physical. The equiprobable three-dimensional distribution of magnetic moments of all particles in space was also taken into account.

The results obtained using the MOTIF program showed that the hyperfine structure parameters of the studied  $\epsilon$ - $\text{Fe}_2\text{O}_3$  nanoparticles are in good agreement with Mössbauer spectroscopy data. The magnetic transition in the range of 80–150 K seen in Fig. 3 is characterized by a sharp increase in the iron hyperfine field ( $H_{\text{hf}}$ ) in tetrahedral positions (Fe4). The resulting temperature dependence  $H_{\text{hf}}(T)$  agrees well with previously known results [10, 19, 22]. The increase in the hyperfine field on Fe4 iron nuclei is accompanied by an order-of-magnitude decrease in the coercive force, which increases again at 4 K almost to the initial values [12, 23]. This behavior correlates with a change in the nonzero orbital angular momentum of iron in this position detected by X-ray magnetic circular dichroism measurements [11]. This orbital angular momen-

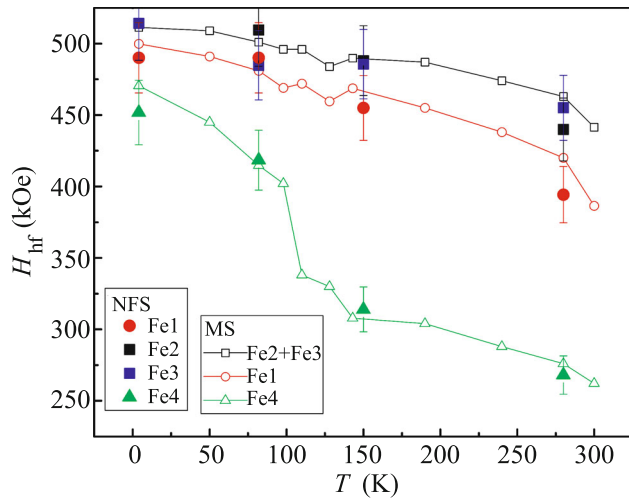


**Fig. 3.** (Color online) Temperature dependence of the hyperfine field  $H_{\text{hf}}$  of ultrasmall  $\epsilon\text{-Fe}_2\text{O}_3$  nanoparticles. Mössbauer and nuclear forward scattering data are shown by open and closed symbols, respectively.

tum is due to the crystallographic distortions of the lattice, which can be considered as a reason for the magnetic transition.

The presence of the nonzero orbital angular momentum of the  $\text{Fe}^{3+}$  cation in the  $\epsilon\text{-Fe}_2\text{O}_3$  structure is an interesting fact. It is logical to assume that the orbital angular momentum of trivalent iron is explained by the admixture effect of oxygen  $2p$  electrons to iron  $e_g$  orbitals, which have a lower energy in a tetrahedral environment. A sharp increase in local distortions in tetrahedral positions leads to the divergence of the energy of  $e_g$  orbitals. Thus, the probability of electron hopping to these orbitals decreases, and the induced orbital angular momentum of iron in tetrahedral positions will decrease, which was shown in experiments [11]. On the contrary, the effective magnetic moment caused by this process will increase, which explains the increase in  $H_{\text{hf}}$  (Fig. 3) owing to an increase in the polarization of inner  $S$ -shell electrons of iron.

The change in the orbital angular momentum in the process of the magnetic transition should change the spin–orbit coupling; as a result, the direction of the magnetic moment will deviate from the quantization axis. This will be manifested in the hyperfine structure as a change in the quadrupole shift ( $QS$ ), since the resulting electric field gradient on the nucleus is produced by the crystal field and the electron shell of the atom itself. Moreover, the contribution of the latter in the case of a spherically symmetric  $\text{Fe}^{3+}$  cation can be ignored. The electric hyperfine interaction between the quadrupole moment of a nucleus with the nuclear spin  $I = 3/2$  and the acting

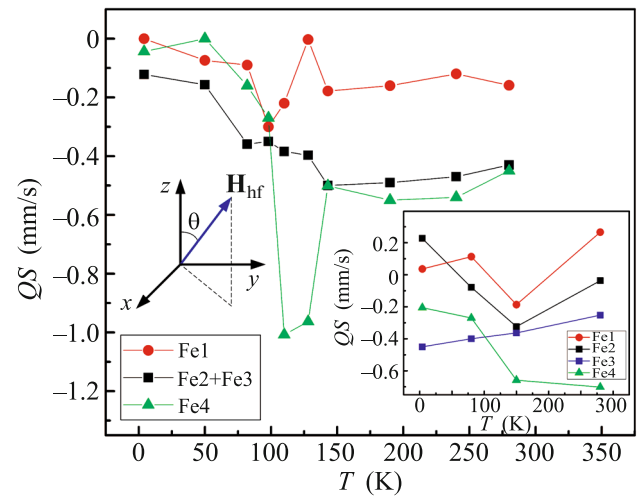


**Fig. 4.** (Color online) Temperature dependence of the quadrupole shift  $QS(T)$  of  $\epsilon\text{-Fe}_2\text{O}_3$  according to Mössbauer spectroscopy data. The inset shows nuclear forward scattering data.

electric field gradient in the case of the axial symmetry is described by the expression

$$\Delta E_Q = \frac{e^2}{4} QV_{zz} \frac{1}{2} (3\cos^2\Theta - 1). \quad (1)$$

Here,  $Q$  is the nuclear quadrupole moment,  $V_{zz}$  is the principal component of the electric field gradient tensor, and  $\Theta$  is the angle between the direction of the electric field gradient and the hyperfine field (Fig. 4). Since the magnetic transition does not change the quadrupole moment of the nucleus, the change in the angle in the magnetic transition can be estimated from the values known from the nuclear forward scattering and Mössbauer spectroscopy data at 80 and 150 K. After excluding the nuclear quadrupole moment from the expression, the change in the angle of the magnetic moment with respect to the direction of the electric field gradient at the magnetic transition in the interval of 150–80 K obtained from our estimates is  $44^\circ$ .

We consider in more detail the temperature behavior of the quadrupole shift of the particles in a locked state, according to the Mössbauer spectroscopy and nuclear forward scattering data (inset of Fig. 4). Qualitatively, the behavior of these  $QS(T)$  dependences coincides. Both sets of dependences have a number of features. The first thing to note is a sharp change in the  $QS$  value in iron positions with a tetrahedral environment at the magnetic transition in the range of 80–150 K, which we associated with a change in the direction of the magnetic moment with respect to the electric field gradient. A  $QS$  jump in the Fe1 position (circles in Fig. 4) indicates a strong coupling between the iron cations inside the layer formed by cations with the undistorted tetrahedral and octahedral oxygen environment. The refinement of the nuclear forward

scattering data by additional temperature points, according to the measurements of the Mössbauer spectra, made it possible to show for the first time that the character of the change in the quadrupole shift in the particles coincides with the character of the change in the orbital angular momentum in  $\epsilon$ -Fe<sub>2</sub>O<sub>3</sub> obtained from X-ray magnetic circular dichroism data [11]. In this case, such a correlation was not observed earlier on larger particles (~25 nm) [10, 22].

#### 4. CONCLUSIONS

In this work, the nuclear  $\gamma$ -resonance methods with the <sup>57</sup>Co(Rh) radioactive source and the synchrotron radiation source on the ID18 beamline at the ESRF in the temperature range of 4–300 K have been applied to study the magnetic transition in  $\epsilon$ -Fe<sub>2</sub>O<sub>3</sub> nanoparticles. The energy and time resolved measurements have been carried out. Highly sensitive nuclear  $\gamma$ -resonance methods have provided important information on the evolution of the magnetic structure during the magnetic transition in the temperature range of 80–150 K. Both methods have shown a sharp increase in the hyperfine field in tetrahedrally coordinated iron regions. This leads to the change in the intensity of the beats on the nuclear forward scattering spectra with a periodicity of ~30 ns and a shift in the first beat to lower times. The magnetic transition has been observed as a separation of nuclear forward scattering spectral peaks in the range of 20–170 ns. The correlation of the quadrupole shift and the orbital angular momentum of iron has been shown in  $\epsilon$ -Fe<sub>2</sub>O<sub>3</sub> nanoparticles for the first time. According to Mössbauer spectroscopy, the magnetic transition is accompanied by the rotation of the magnetic moment of iron in the tetrahedral positions around the axis of the electric field gradient by an angle of 44°. Such correlation has not been observed in larger  $\epsilon$ -Fe<sub>2</sub>O<sub>3</sub> nanoparticles. Thus, the increase in the surface effects apparently shifts the magnetic moments with respect to the axis of the electric field gradient in  $\epsilon$ -Fe<sub>2</sub>O<sub>3</sub> nanoparticles. A more detailed study of the magnetic structure can be carried out in nuclear forward scattering experiments with an external magnetic field.

#### ACKNOWLEDGMENTS

Nuclear forward scattering spectra were obtained within the SC-4708 experiment at the European Synchrotron Radiation Facility.

#### FUNDING

This work was supported by the Russian Science Foundation (project no. 17-12-01111).

#### REFERENCES

1. Yu. V. Shvyd'ko, S. L. Popov, and G. V. Smirnov, *JETP Lett.* **53**, 217 (1991).

2. R. Rüffer and A. I. Chumakov, *Hyperfine Interact.* **97**, 589 (1996).
3. R. Röhlberger, J. Bansmann, V. Senz, K. L. Jonas, A. Bettac, K. H. Meiwes-Broer, and O. Leupold, *Phys. Rev. B* **67**, 245412 (2003).
4. E. Bykova, L. Dubrovinsky, N. Dubrovinskaya, M. Bykov, C. McCammon, S. V. Ovsyannikov, H. P. Liermann, I. Kuznetsov, A. I. Chumakov, R. Rüffer, M. Hanfland, and V. Prakapenka, *Nat. Commun.* **7**, 10661 (2016).
5. M. Mikolasek, K. Ridier, D. Bessas, V. Cerantola, G. Félix, G. Chaboussant, M. Piedrahita-Bello, E. Angulo-Cervera, L. Godard, W. Nicolazzi, L. Salmon, G. Molnár, and A. Bousseksou, *J. Phys. Chem. Lett.* **10**, 1511 (2019).
6. J. L. García-Muñoz, A. Romaguera, F. Fauth, J. Nogués, and M. Gich, *Chem. Mater.* **29**, 9705 (2017).
7. I. Sergueev, A. I. Chumakov, T. D. Beaume-Dang, R. Rüffer, C. Strohm, and U. van Bürck, *Phys. Rev. Lett.* **99**, 097601 (2007).
8. M. Herlitschke, S. Disch, I. Sergueev, K. Schlage, E. Wetterskog, L. Bergström, and R. P. Hermann, *J. Phys.: Conf. Ser.* **711**, 012002 (2016).
9. J. Tuček, P. Tuček, J. Čuda, J. Filip, J. Pechoušek, L. Machala, and R. Zbořil, *AIP Conf. Proc.* **1489**, 56 (2012).
10. M. Gich, C. Frontera, A. Roig, E. Taboada, E. Molins, H. R. Rechenberg, J. D. Ardisson, W. A. A. Macedo, C. Ritter, and V. Hardy, *Chem. Mater.* **18**, 3889 (2006).
11. Y.-C. Tseng, N. M. Souza-Neto, D. Haskel, M. Gich, C. Frontera, A. Roig, M. van Veenendaal, and J. Nogués, *Phys. Rev. B* **79**, 094404 (2009).
12. D. A. Balaev, A. A. Dubrovskiy, K. A. Shaykhtudinov, O. A. Bayukov, S. S. Yakushkin, G. A. Bukhtiyarova, and O. N. Mart'yanov, *J. Appl. Phys.* **114**, 163911 (2013).
13. Yu. V. Knyazev, D. A. Balaev, V. L. Kirillov, O. A. Bayukov, and O. N. Mart'yanov, *JETP Lett.* **108**, 527 (2018).
14. E. Tronc, C. Chanéac, J. P. Jolivet, and J. M. Grenèche, *J. Solid State Chem.* **139**, 93 (1998).
15. S. S. Yakushkin, D. A. Balaev, A. A. Dubrovskiy, S. V. Semenov, Yu. V. Knyazev, O. A. Bayukov, V. L. Kirillov, R. D. Ivantsov, I. S. Edelman, and O. N. Mart'yanov, *Ceram. Int.* **44**, 17852 (2018).
16. G. V. Smirnov, *Hyperfine Interact.* **125**, 91 (2000).
17. A. Q. R. Baron, *Hyperfine Interact.* **125**, 29 (2000).
18. Yu. V. Shvyd'ko, *Hyperfine Interact.* **123**, 275 (1999).
19. A. A. Dubrovskiy, D. A. Balaev, K. A. Shaykhtudinov, O. A. Bayukov, O. N. Pletnev, S. S. Yakushkin, G. A. Bukhtiyarova, and O. N. Mart'yanov, *J. Appl. Phys.* **118**, 213901 (2015).
20. J.-L. Rehspringer, S. Vilminot, D. Niznansky, K. Záveta, C. Estournes, and M. Kurmoo, *Hyperfine Interact.* **166**, 475 (2005).
21. S. Mørup and H. Topsoe, *Appl. Phys.* **11**, 63 (1976).
22. J. Kohout, P. Brázda, K. Záveta, D. Kubániová, T. Kmječ, L. Kubíčková, M. Klementová, E. Šantavá, and A. Lančok, *J. Appl. Phys.* **171**, 17D505 (2015).
23. M. Gich, A. Roig, C. Frontera, E. Molins, J. Sort, M. Popovici, G. Chouteau, D. Martín y Marero, and J. Nogués, *J. Appl. Phys.* **98**, 044307 (2005).

*Translated by L. Mosina*